

# SDSS J0025-10 at $z=0.30$ : a (U)LIRG to optical QSO transition candidate <sup>\*</sup>

M. Villar-Martín<sup>1</sup>, B. Emonts<sup>2,1</sup>, M. Rodríguez<sup>3</sup>, M. Pérez Torres<sup>3</sup>, G. Drouart<sup>4,5</sup>

<sup>1</sup> *Centro de Astrobiología (INTA-CSIC), Carretera de Ajalvir, km 4, 28850 Torrejón de Ardoz, Madrid, Spain. villarmm@cab.inta-csic.es*

<sup>2</sup> *CSIRO Astronomy and Space Science, Australia Telescope National Facility, PO Box 76, Epping NSW 1710, Australia*

<sup>3</sup> *Instituto de Astrofísica de Andalucía (CSIC), Glorieta de la Astronomía s/n, 18008 Granada, Spain*

<sup>4</sup> *European Southern Observatory (ESO), Karl Schwarzschild Str. 2, D-85748, Garching bei München, Germany*

<sup>5</sup> *Institut d'Astrophysique de Paris (IAP), 98B Boulevard Arago, 75014 Paris, France*

Accepted 2013 March 25. Received 2013 March 15; in original form 2012 November 15

## ABSTRACT

We have characterized the amount, spatial distribution and kinematics of the molecular gas in the merging, double nucleus type 2 quasar SDSS J0025-10 at  $z=0.30$  using the CO(1-0) transition, based on data obtained with the Australia Telescope Compact Array (ATCA). This is one of the scarce examples of quasar host galaxies where the CO emission has been resolved spatially at any redshift. We infer a molecular gas mass  $M_{\text{H}_2}=(6\pm 1)\times 10^9 M_{\odot}$ , which is distributed in two main reservoirs separated by  $\sim 9$  kpc.  $\sim 60\%$  of the gas is in the central region, associated with the QSO nucleus and/or the intermediate region between the two nuclei. The other 40% is associated with the northern tidal tail and is therefore unsettled.

With its high infrared luminosity  $L_{\text{IR}}=(1.1\pm 0.3)\times 10^{12} L_{\odot}$ , SDSS J0025-10 is an analogue of local luminous LIRGs and ULIRGs. On the other hand, the clear evidence for an ongoing major merger of two gas rich progenitors, the high  $L_{\text{IR}}$  dominated by a starburst, the massive reservoir of molecular gas with a large fraction still unsettled, and the quasar activity are all properties consistent with a transition phase in the (U)LIRG-optical QSO evolutionary scenario. We propose that we are observing the system during a particular transient phase, prior to more advanced mergers where the nuclei have already coalesced.

We argue that a fraction of the molecular gas reservoir is associated with a tidal dwarf galaxy identified in the optical Hubble Space Telescope image at the tip of the northern tidal tail. The formation of such structures is predicted by simulations of colliding galaxies.

**Key words:** galaxies:evolution; galaxies:interactions; quasars:individual: SDSS J002531.46-104022.2

## 1 INTRODUCTION

CO studies of type 1 quasars (QSO1) at different  $z$  have provided accumulating evidence that they often contain an abundant supply of molecular gas. At redshift  $z < 0.5$ , the range of molecular gas masses spans at least two orders of magnitude: some quasars have  $M_{\text{H}_2} \lesssim 10^8 M_{\odot}$  significantly lower than the Milky Way (few  $\times 10^9 M_{\odot}$ ) and others contain giant reservoirs  $> 10^{10} M_{\odot}$ . At the high redshift ( $z > 2$ ), quasars contain  $M_{\text{H}_2} \sim \text{several} \times 10^9$  to  $\sim 10^{11} M_{\odot}$  (e.g. Bertram et al. 2007, Xia et al. 2012). As found for other

galaxy types, these works show that quasars with the highest infrared luminosities also contain the largest  $M_{\text{H}_2}$ .

The investigation of the molecular gas content of type 2 quasars (QSO2)<sup>1</sup> has been quite active in recent years, although almost invariably focussed on high  $z > 2$  objects (e.g. Martínez Sansigre et al. 2009) and with scarce spatial information.

Regarding studies of the molecular gas content of quasars in general, the intermediate redshift range ( $0.1 \lesssim z \lesssim 1.5$ ) has remained practically unexplored until very recently (Xia et al. 2012, Krips, Neri & Cox 2012, Villar-

<sup>\*</sup> Based on observations carried out with the Australia Telescope Compact Array

<sup>1</sup> We refer to QSO2 as radio quiet objects, as opposite to narrow line radio galaxies

Martín et al. 2013). This redshift range spans  $\sim 60\%$  of the age of the Universe, an epoch of declining cosmic star formation rate (Hopkins & Beacom 2006). Results for QSO2 at redshift  $z < 0.5$  have been published only in the last year (Krips, Neri & Cox 2012, Villar-Martín et al. 2013). They suggest that QSO2 often harbor large reservoirs of molecular gas ( $\sim \text{several} \times 10^9 M_{\odot}$ ), similar to QSO1 of similar IR luminosity.

Detailed studies of the spatial distribution of the molecular gas in quasar host galaxies is of special interest. This gas is highly sensitive to the different mechanisms at work during galactic evolution. As such, it retains relic information about the global history of the systems. The spatial redistribution of the molecular gas during the interactions/merger processes is determinant on the triggering of the starburst and (probably) the quasar activities (Bessiere et al. 2012, Ramos Almeida et al. 2011), while powerful negative feedback might be able to counteract this by cleaning and/or destroying the molecular gas reservoirs and so quenching the star formation and quasar activities (Hopkins & Beacom 2006).

Such studies are very scarce and have also mostly focussed on the highest redshift QSO1 (e.g. Carilli et al. 2002). The main reasons have been so far the lack in sensitivity and the narrow bandwidths of (sub)-mm telescopes as well as the major interest on the most distant sources. Spatially resolved data on QSO in the local and intermediate redshift ( $z < 1.5$ ) universe are also limited in number (e.g. Feruglio et al. 2010, Aravena et al. 2011, Papadopoulos et al. 2008, Krips et al. 2007, Staguhn et al. 2004). The results so far indicate that a large fraction of the molecular gas in low  $z$  quasars (as well as in luminous [ $10^{11} \leq L_{\text{IR}}/L_{\odot} < 10^{12}$ ] and ultraluminous [ $10^{12} \leq L_{\text{IR}}/L_{\odot} < 10^{13}$ ] infrared galaxies, LIRGs and ULIRGs) is highly concentrated in the galactic centers, most frequently in rotating disks and rings of  $\lesssim$  few kpc diameter (e.g. Westmoquette et al. 2012, Bryant & Scoville 1999). At intermediate  $z$ , some systems have extended and massive reservoirs of molecular gas, associated with companion objects and/or tidal structures (Aravena et al. 2011, Papadopoulos et al. 2008).

We present here a detailed study of the spatial distribution of the molecular gas traced by the CO(1-0) transition in SDSS J002531.46-104022.2 (SDSS J0025-10 hereafter), a QSO2 at  $z=0.303$  selected from Sloan Digital Sky Survey (SDSS) database. The CO(1-0) ( $\nu_{\text{rest}}=115.27$  GHz) transition is the least dependent on the excitation conditions of the gas, which is crucial for deriving reliable estimates of the total molecular gas content, including the wide-spread, low-density gas that may be sub-thermally excited (e.g. Papadopoulos et al. 2001, Carilli et al. 2010).

SDSS J0025-10 has special interest since it is undergoing a strong transformation via a major merger event and allows to investigate the distribution and dynamics of the molecular gas during the process. It moreover shows evidence for phenomena frequently found in quasars which can have a profound impact on the evolution of their hosts: mergers/interactions, star formation and nuclear outflows. A complete study of this system requires the quantification of the molecular gas content and the characterization of its spatial distribution and kinematics. This is the purpose of this paper.

## 1.1 SDSS J0025-10

Villar-Martín et al. (2011a, 2011b, VM11a and VM11b hereafter) present a detailed study of this system based on deep optical imaging and spectroscopic data obtained with the Faint Object FOCal Reducer and low dispersion Spectrograph (FORs2) on the Very Large Telescope (VLT). Based on the high [OIII] $\lambda 5007$  luminosity ( $\log(\frac{L_{[\text{OIII}]}}{L_{\odot}})=8.73$ ) and other criteria related to the optical emission line ratios and widths, the object was classified as a QSO2 by Zakamska et al. (2003). This QSO2 is a member of an interacting system. It has two nuclei located at  $\sim 5$  kpc in projection. The velocity shift  $\Delta V=-20 \pm 20$  km  $s^{-1}$  between them implied by the optical spectrum (VM11a), is consistent with their relative motion being approximately constrained on the plane of the sky and thus, the apparent separation is similar to the true separation. One nucleus hosts the quasar and the other is forming stars actively. Tidal tails stretch to the North and South. Their predominance in the broad band optical images shows that they are dominated by stellar continuum emission, although line emission from ionized gas is also detected.

The optical emission line spectra reveal extended recent star formation in the companion nucleus (that sometimes we will refer to as *nuc2*) and the northern tidal tail. Since only stars with masses of  $>10 M_{\odot}$  and lifetimes of  $<20$  Myr contribute significantly to the integrated ionizing flux, this sets an upper limit on the age of the most recent burst of star formation at these locations. Moreover, compact knots that are visible in the tidal tail (see Hubble Space Telescope (HST) image in Villar Martín et al. 2012) are reminiscent of star clusters and/or tidal dwarf galaxies. The presence of a young stellar population ( $<40$  Myr) in the quasar nucleus is also confirmed by fits of the spectral energy distribution (SED) of the optical continuum (Bessiere et al. 2013, in prep.).

The quasar nucleus hosts an ionized outflow of uncertain origin (AGN and/or starburst induced), which produces very broad emission line components with full width half maximum FWHM  $\sim 1300$  km  $s^{-1}$  and blueshifted by  $\sim 80$  km  $s^{-1}$  relative to the systemic redshift of the galaxy (VM11b).

We assume  $\Omega_{\Lambda}=0.7$ ,  $\Omega_{\text{M}}=0.3$ ,  $H_0=71$  km  $s^{-1}$  Mpc $^{-1}$ . At  $z=0.303$ ,  $1''$  corresponds to 4.45 kpc.

## 2 ATCA OBSERVATIONS AND HST ARCHIVE DATA

The observations were performed during 2-7 August 2012 with the Australia Telescope Compact Array (ATCA), a radio interferometer in Narrabri, Australia. The ATCA was configured in the most compact hybrid H75 array configuration. Two 2 GHz bands with 1 MHz channel resolution were centered on the redshifted frequency of the CO(1-0) line (88.439 GHz), providing redundancy in case technical issues would occur with one of the bands. This resulted in a velocity coverage of 7000 km  $s^{-1}$ , maximum resolution of 3.5 km  $s^{-1}$  and primary telescope beam (i.e. effective field-of-view) of 32 arcsec. Observations were done above an elevation of  $35^{\circ}$  and under good weather conditions, with system temperatures ranging between 450 and 800 K (depending on the antenna and the elevation of the source) and

typical atmospheric seeing fluctuations  $< 150 \mu\text{m}$  (phase de-correlation of  $< 10\%$ , see Middelberg, Sault & Kesteven 2006). The total on-source integration time was 17 hours.

The phases and bandpass were calibrated every 7.5 minutes with a short ( $\sim 2$  min) scan on the nearby bright calibrator PKS 0003-066 ( $S_{88.4\text{GHz}} = 1.8 \text{ Jy}$  at 88.4 GHz), located at  $6.4^\circ$  distance from our target source. Atmospheric amplitude variation were calibrated every 30 minutes using a paddle scan, and telescope pointing was updated every hour, or every time the telescope moved  $> 20^\circ$  on the sky. For absolute flux calibration, Uranus was observed close to our target source.

The off-line data reduction was done with the MIRIAD software (Sault, Teuben & Wright 1995). Bad data (including data with internal interference or shadowing of an antenna, or data taken during weather conditions that introduced significant phase decorrelation) were discarded. PKS 0003-066 was used for both phase as well as time-dependent bandpass calibration by interpolating the calibration solution obtained every 7.5 minutes (see Emonts et al. 2011 for details on time-dependent bandpass calibration within MIRIAD). Atmospheric opacity variations were corrected by weighting the data according to their ‘above atmosphere’ (i.e. paddle-corrected) system temperature. Flux calibration was applied using Uranus [ATCA Uranus model version Aug 2012], resulting in an absolute flux calibration accuracy of 20%. After Fourier transformation, we obtained a data cube with robust weighting +1 (Briggs 1995). The data presented in this paper were binned by 10 channels and subsequently Hanning smoothed to a velocity resolution of  $68 \text{ km s}^{-1}$ , yielding a noise level of  $0.7 \text{ mJy beam}^{-1} \text{ chan}^{-1}$ . The synthesized beam-size of the data is  $6.30 \times 4.39 \text{ arcsec}^2$  (PA  $-85.3^\circ$ ). Total intensity images were created by summing all the signal (i.e. without setting a noise threshold) across the velocity ranges in which CO(1-0) was detected. The calculated CO luminosities in this paper have been derived from these total intensity images (see § 3.1).

No 88.4 GHz radio continuum was detected in the data down to a  $5\sigma$  limit of 0.5 mJy.

The HST image, which was obtained with the ACS/WFC (Advanced Camera for Surveys/Wide Field Camera), was retrieved from the HLA (Hubble Legacy Archive; programme identification 10880 and principal investigator H. Scmitt). The only processing applied was cosmic ray removal. The accuracy of the HST astrometry is  $\sim 0.3''$  in both coordinates. The accuracy of the CO astrometry is expected to be significantly smaller ( $\lesssim 0.1''$ ; see e.g. Papadopoulos et al. 2008).

### 3 RESULTS

#### 3.1 SDSS J0025-10 is a (U)LIRG

We have constrained the infrared (IR) luminosity,  $L_{\text{IR}}$  (inferred from the 8-1000  $\mu\text{m}$  wavelength range) by fitting the source spectral energy distribution (SED) defined by the Wide-Field Infrared Explorer (WISE; 3.3, 4.6, 11.6, 22.1  $\mu\text{m}$ ) and Infrared Astronomical Satellite (IRAS; 60 and 100  $\mu\text{m}$ ) photometric measurements, as well as the upper limit on the  $\sim 3 \text{ mm}$  continuum measured with the ATCA data (see Fig.1). Optical photometry has not been used, since this

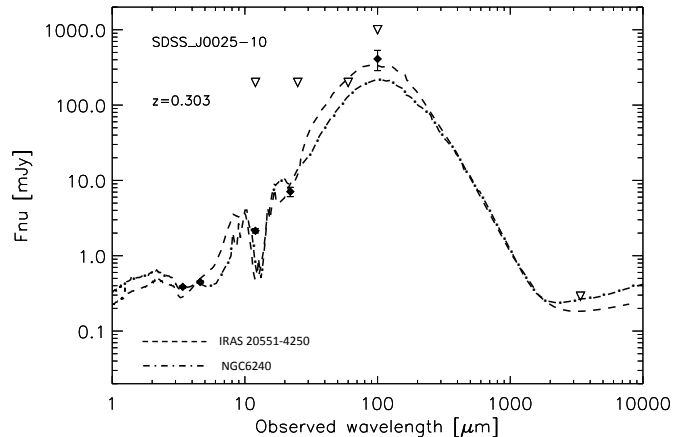


**Figure 1.** Fit of the near to far infrared SED of SDSS J0025-10 based on WISE and IRAS photometry and the ATCA 3mm continuum upper limit. Detections and upper limits are marked with diamonds and triangles respectively. Different line styles are used for the two SEDs discussed in the text.

band is known to be a complex mixture of stellar and AGN related components (scattered and/or direct AGN light and nebular continuum; e.g. Tadhunter et al. 2011, Vernet et al. 2001). To build the SED we used the SWIRE template library (Polletta et al. 2008) which contains 25 templates including ellipticals, spirals, starbursts, type 2 and type 1 AGN and composite starburst + AGN.

The best fit corresponds to the starburst template IRAS 20551-4250 (Fig. 1, dashed line). We infer  $L_{\text{IR}} = (1.4 \pm 0.4) \times 10^{12} L_{\odot}$  for this SED. The starburst template NGC 6240, which also produces a reasonable fit, is also shown for illustration (Fig. 1, dot-dashed line) because this LIRG system is similar in many aspects to SDSS J0025-10 (double nuclei, interacting local LIRG, Tecza et al. 2000, Tacconi et al. 1999). For this SED,  $L_{\text{IR}} = (8.2 \pm 0.2) \times 10^{11} L_{\odot}$ .

With these two SEDs we constrain the infrared luminosity  $L_{\text{IR}} = (1.1 \pm 0.3) \times 10^{12} L_{\odot}$ . Taking the uncertainties into account, SDSS J0025-10 is in the transition range of  $L_{\text{IR}}$  values between the LIRG and the ULIRG regimes.

The fits show that the infrared luminosity of SDSS J0025-10 is dominated by a starburst. We calculate the star forming rate as  $\text{SFR} = 1.73 \times 10^{-10} \times L_{\text{IR}} (M_{\odot} \text{ yr}^{-1}) = 190 \pm 52 M_{\odot} \text{ yr}^{-1}$ , assuming solar abundances and a Salpeter Initial Mass Function (IMF) (Kennicutt 1998).

#### 3.2 Mass and spatial distribution of the molecular gas

We measure a total CO(1-0) luminosity in SDSS J0025-10 of  $L'_{\text{CO}} = (7.5 \pm 1.5) \times 10^9 \text{ K km s}^{-1} \text{ pc}^2$ .  $L'_{\text{CO}}$  is calculated as:

$$L'_{\text{CO}} = 3.25 \times 10^7 \left( \frac{S_{\text{CO}} \Delta V}{\text{Jy km/s}} \right) \left( \frac{D_L}{\text{Mpc}} \right)^2 \left( \frac{\nu_{\text{rest}}}{\text{GHz}} \right)^{-2} (1+z)^{-1}$$

where  $I_{\text{CO}} = S_{\text{CO}} \Delta V$  is the integrated CO(1-0) line intensity in  $\text{Jy km s}^{-1}$ ,  $D_L$  is the luminosity distance in Mpc and  $\nu_{\text{rest}} = 115.27 \text{ GHz}$ , is the rest frame frequency of the CO(1-0) transition (Solomon & Vanden Bout 2005). With this  $L'_{\text{CO}}$ , the system follows the  $L'_{\text{CO}}$  vs.  $L_{\text{IR}}$  (or

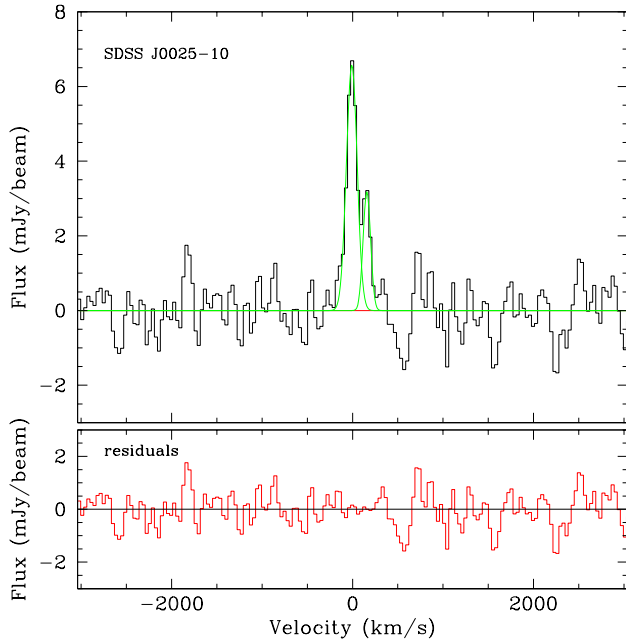


**Figure 2.** 1-dimensional spectrum of SDSS J0025-10, extracted against the QSO2 nucleus ( $2.3'' \times 2.3''$ ). Notice the double horned profile, with Gaussian fits visualizing the two components described in the text. The bottom plot shows the residuals after subtracting the two Gaussian profiles from the spectrum. Velocity values are relative to the peak of the ‘blue’ component, which we assume as the systemic velocity ( $z=0.3031 \pm 0.0001$ , see text).

$L_{\text{FIR}}$ ) correlation defined by different types of galaxies (Solomon & Vanden Bout 2005), including QSO1 and QSO2 (Bertram et al. 2007, Villar-Martín et al. 2013, Krips, Neri & Cox 2012). The molecular gas mass is then calculated as  $M_{\text{H}_2} = \alpha \times L'_{\text{CO}} = (6 \pm 1) \times 10^9 M_{\odot}$ , assuming  $\alpha = 0.8 L_{\odot} (\text{K km s}^{-1} \text{ pc}^2)^{-1}$ . This value of  $\alpha$  is often used in studies of (U)LIRGs and active galaxies (e.g. Downes & Solomon 1998), although a range  $\alpha \sim 0.3\text{--}1.3$  is possible (e.g. Solomon & van den Bout 2005, Sanders & Mirabel 1996). Similar amounts of molecular gas have been measured for quasars (both type 1 and type 2) of similar infrared luminosity and redshift (e.g. Krips, Neri & Cox 2012, Villar-Martín et al. 2013).

The CO(1-0) line shows a double horned profile (Fig. 2) with two kinematic components. The blue component has  $z = 0.3031 \pm 0.0001$  (which we assume as the systemic redshift  $z_{\text{sys}}$ ) and  $\text{FWHM} = 140 \pm 25 \text{ km s}^{-1}$ . The red, fainter component is shifted by  $+160 \pm 10 \text{ km s}^{-1}$  and has  $\text{FWHM} = 80 \pm 40 \text{ km s}^{-1}$ . A negative depression (around  $v = 500 \text{ km s}^{-1}$ ) is also visible in Fig. 2. This feature appears at  $-2.8\sigma$  (when integrated over its full extent). Fig. 2 (bottom) shows that it may be merely a prominent noise peak in the data. Since this negative depression is not noticeably caused by external effects (e.g. weather or phase calibration), it may also indicate that there are low-level systematics affecting the ATCA 3mm (similar to low-level systematics described by Emonts et al. 2011 that occur at the extreme edge of the ATCA 7mm band, or possible baseline artifacts mentioned by Norris et al. (2013) in early wide-band 3mm ATCA data). Regardless, the integrated blue and red part of the double horned CO profile are detected at the  $10\sigma$  and

$7\sigma$  significance level respectively and thus unambiguously stand out above the noise, indicating the reliability of the CO emission discussed in this paper.

The spatial distribution of CO(1-0) in different channel maps is shown in Fig. 3 overlaid on the HST optical image. The CO(1-0) emission detected at  $\geq 3\sigma$  level spans a range of velocities  $\sim [-110, +230] \text{ km s}^{-1}$  relative to  $z_{\text{sys}}$ . The CO(1-0) is spatially extended and accumulated in two main reservoirs separated by  $\sim 2''$  or  $\sim 9 \text{ kpc}$  (blue and red contours in Fig. 3, first panel) which we will name J0025A and J0025B. The similarity within the errors of the velocity shift between them, compared to the two kinematic components isolated on the 1-dimensional spectrum suggests that J0025A and J0025B are responsible for the double horned profile discussed above. J0025A and J0025B have CO luminosities of  $(4.3 \pm 0.9) \times 10^9$  and  $(3.1 \pm 0.9) \times 10^9 \text{ K km s}^{-1} \text{ pc}^2$  respectively<sup>2</sup>, which correspond to  $M_{\text{H}_2} = (3.4 \pm 0.7) \times 10^9$  and  $(2.5 \pm 0.7) \times 10^9 M_{\odot}$ .

In Fig. 4 we show the location of the peaks of the CO(1-0) emission in J0025A and J0025B overlaid onto the HST image. These locations have been derived by fitting a Gaussian profile to the integrated CO(1-0) emission. Within the uncertainty, this Gaussian profile could be represented by a point source with the size of the synthesized beam. The locations of the CO(1-0) peaks in the different channel maps of Fig. 3 are also plotted, including the uncertainty due to fitting and astrometric errors (see caption for details). From Fig. 4 it is clear that the CO(1-0) emission in J0025B is associated with the northern tidal tail while J0025A is preferentially associated with the QSO2 nucleus and/or the region *between* both nuclei.

We do not detect any CO(1-0) emission associated with the companion nucleus *nuc2*. However, the star forming activity it harbours (§1.1) requires a local supply of molecular gas. The  $\text{H}\beta$  luminosity from *nuc2* (VM11a) implies a line reddening corrected  $\text{SFR} \sim 8 M_{\odot} \text{ yr}^{-1}$ , assuming  $\text{SFR}(M_{\odot} \text{ yr}^{-1}) = 2.3 \times 10^{-41} \frac{L_{\text{H}\beta}}{\text{ergs}^{-1}}$  for solar abundances and a Salpeter IMF (Kennicutt 1998).<sup>3</sup> This in turns implies  $L_{\text{IR } nuc2} \sim 4.6 \times 10^{10} L_{\odot}$ , which would be a lower limit if part of the star formation were totally obscured (Rodríguez Zaurín et al. 2011). This is  $\sim 8\%$  of the total  $L_{\text{IR}}$  of the system. If *nuc2* follows the  $L_{\text{IR}}$  vs.  $L'_{\text{CO}}$  correlation defined by star forming galaxies (see Fig. 8 in Solomon & van den Bout 2005), it roughly implies that it contains  $\gtrsim 8\%$  of the total molecular gas or  $\gtrsim 5 \times 10^8 M_{\odot}$ . The  $3\sigma$  upper limit for a CO(1-0) non-detection with  $\text{FWHM} = 140 \text{ km s}^{-1}$  in our data is  $L'_{\text{CO}} = 1.0 \times 10^9 \text{ K km s}^{-1} \text{ pc}^2$ , or  $M_{\text{H}_2} = 8 \times 10^8 M_{\odot}$ . Although the calculations are highly uncertain due to the large scatter of the  $L_{\text{IR}}$  vs  $L'_{\text{CO}}$  correlation and the uncertainty on the amount of obscured star formation in *nuc2*, they imply that its CO(1-0) emission likely falls below the detection limit of our data (or otherwise a low-level signal

<sup>2</sup> Values have been derived from the total intensity image in Fig. 3, but were corrected for line contamination and missed low-level flux based on the Gaussian fitting of the profiles (Fig. 2). This did not significantly change the values for the blue component, but increased both the estimated value and the associated uncertainty of the flux of the red component by 10%. The errors also reflect the 20% uncertainty in absolute flux calibration (§2).

<sup>3</sup> For comparison, the SFR over the entire Milky Way is several  $M_{\odot} \text{ yr}^{-1}$  (e.g. Robitaille & Whitney 2010)

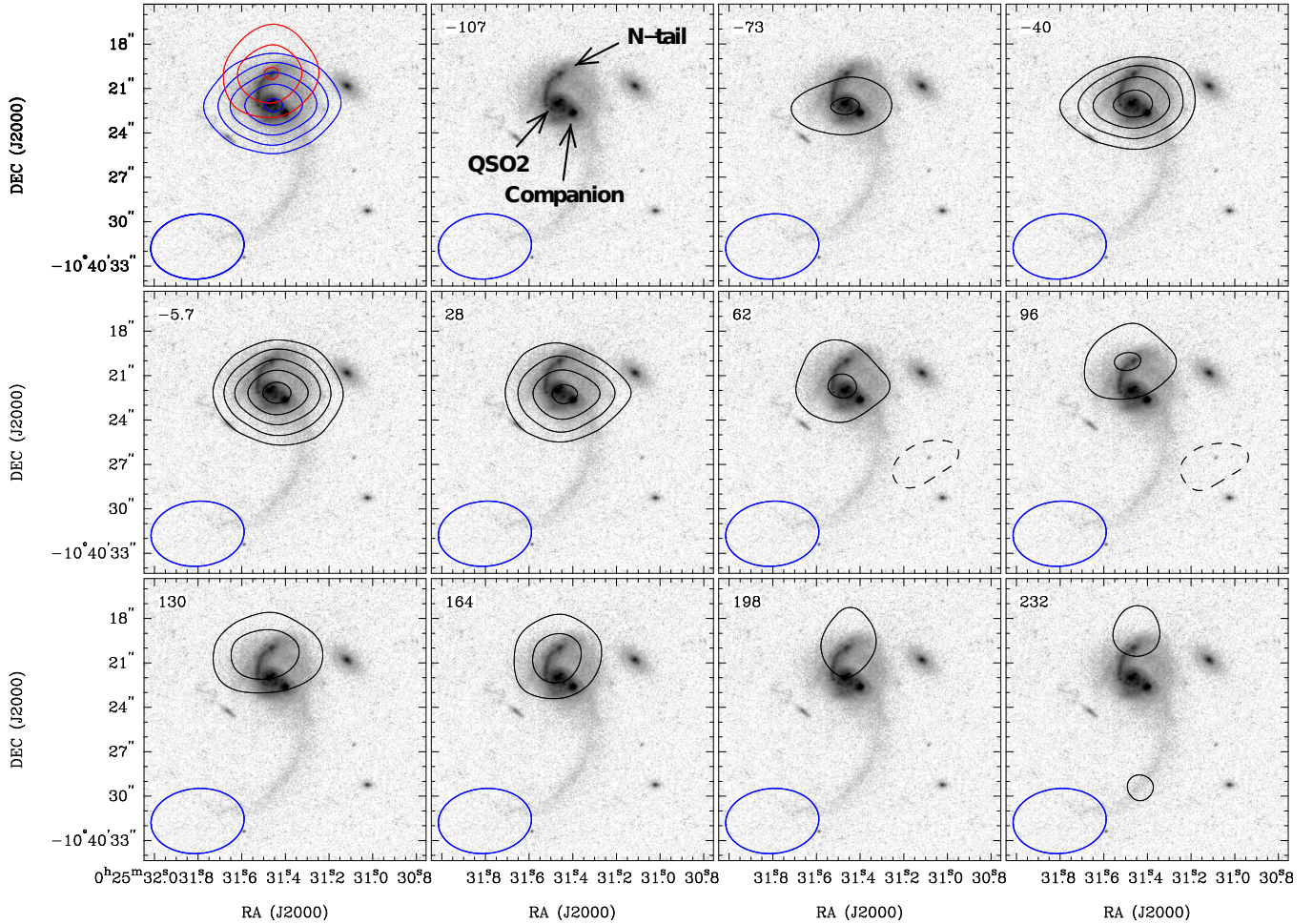


**Figure 3.** The total intensity image of both the blue (J0025A,  $-90 \leq v \leq 79 \text{ km s}^{-1}$ ) and red (J0025B,  $79 \leq v \leq 249 \text{ km s}^{-1}$ ) part of the CO(1-0) signal is shown in the first frame, followed by the channel maps of the CO emission. Contour levels of the total intensity map: 0.27, 0.41, 0.54, 0.68, 0.81  $\text{Jy bm}^{-1} \times \text{km s}^{-1}$ ; contour levels channel maps: -3.0 (dashed), 3.0, 4.5, 6.0, 7.5, 9.0 (solid)  $\times \sigma$ , with  $\sigma = 0.7 \text{ mJy bm}^{-1}$ . Velocity values are relative to  $z_{sys} = 0.3031 \pm 0.0001$ . The location of the QSO2, companion star forming nucleus and the northern tidal tail are indicated in the second panel. A color version of this figure can be seen in the electronic form.

would likely be hidden within the large ATCA beam by the dominant emission from the quasar nucleus and/or intermediate region). New observations with higher spatial resolution and sensitivity are required to both determine the exact location of the CO in J0025A and measure (or set reliable limits on) the CO content of the star forming companion nucleus.

## 4 DISCUSSION

### 4.1 SDSS J0025-10 vs. local (U)LIRGs

SDSS J0025-10 is a (U)LIRG double nuclei merging system with all observed properties consistent with those of numerous local ( $z \lesssim 0.05$ ) luminous LIRGs (several  $\times 10^{11} \lesssim L_{\text{IR}} < 10^{12} L_{\odot}$ ) and ULIRGs. It shows clear morphological evidence for an ongoing major merger: the double nucleus, the tidal tails, the inner spiral structure (which surrounds the QSO nucleus clockwise and apparently becomes the northern tidal tail) and the stellar clusters and/or tidal dwarf

galaxies observed along this structure (Fig. 4) are all morphological features often observed in ULIRGs and luminous LIRGs (Haan et al. 2011, Miralles Caballero et al. 2011, Monreal Ibero et al. 2007). As in these systems, the star formation and probably the AGN activity are triggered by the interaction (see Alonso-Herrero 2013 for a recent review; see also Bessiere et al. 2012).

The IR luminosity,  $L_{\text{IR}} = (1.1 \pm 0.3) \times 10^{12} L_{\odot}$ , which is dominated by the starburst component, the large molecular gas content  $M_{\text{H}_2} = (6 \pm 1) \times 10^9 M_{\odot}$ , the  $\text{SFR} = 190 \pm 52 M_{\odot} \text{ yr}^{-1}$ , the star formation efficiency  $\text{SFE} = \frac{L_{\text{IR}}}{M_{\text{H}_2}} = 183 \pm 62 L_{\odot} M_{\odot}^{-1}$  and the gas exhaustion time scale  $\tau_{\text{SF}} = \frac{M_{\text{H}_2}}{\text{SFR}} = 32 \pm 11 \text{ Myr}$  are all in the range of luminous LIRGs and ULIRGs (Solomon & van den Bout 2005, Sanders & Mirabel 1996, Alonso-Herrero 2013).

In SDSS J0025-10 one nucleus hosts the AGN and both harbour star formation. About 20-30% of local LIRGs have an optically identified AGN, with this percentage increasing with the  $L_{\text{IR}}$  and becoming  $\sim 70\%$  for ULIRGs (e.g. Yuan,

Kewley & Sanders 2010, Nardini et al. 2010, Veilleux et al. 1999, 1995). On the other hand, a large fraction ( $\sim 63\%$ ) of local luminous LIRGs and ULIRGs have double nuclei (Haan et al. 2011) with a variety of scenarios. In some cases both nuclei host star formation and AGN activities (being NGC6240 the most famous example; e.g. Tecza et al. 2000, Tacconi et al. 1999); in others star formation is detected in both nuclei, but none seem to harbour AGN activity or show a composite AGN+starburst spectrum, like SDSS J0025-10 (e.g. Yuan, Kewley & Sanders 2010).

The CO gas in SDSS J0025-10 is distributed in two main spatial components, J0025A and J0025B of masses  $(3.4 \pm 0.7) \times 10^9$  and  $(2.5 \pm 0.7) \times 10^9 M_{\odot}$  respectively. They are separated by  $2''$  or  $\sim 9$  kpc (projected distance) in space and  $160 \text{ km s}^{-1}$  in velocity. J0025A is preferentially associated with the quasar nucleus and/or the intermediate region between the two interacting nuclei, while J0025B is associated with the northern tidal tail. CO(1-0) emission from the companion nucleus is not unambiguously detected, although the active star formation it hosts implies that there must be a local reservoir of  $M_{\text{H}_2} \gtrsim \text{several} \times 10^8 M_{\odot}$ . The CO gas in local (U)LIRGs is usually highly concentrated in the central region towards the core of the merger ( $r \lesssim 1$  kpc, e.g. Bryant & Scoville 1999, Sanders & Mirabel 1996). In addition, a significant fraction of the gas is sometimes spread over scales of 10 kpc or more. This is possibly the case of SDSS J0025-10: J0025A might be the compact, central concentration (although higher spatial resolution observations are required to constrain its exact location and compactness), while J0025B is the more extended gaseous component.

#### 4.2 SDSS J0025-10 as a (U)LIRG-optical QSO transition object

Both theory and observations support that the merger of two gas rich progenitor galaxies form a new, more massive elliptical galaxy (e.g. Toomre & Toomre 1972, Barnes & Hernquist 1996). As a consequence of the gravitational interaction, gaseous dissipation funnels gas into the the gravitational center and triggers intense star formation, which is manifested in the (U)LIRG phenomenon. The gas inflow could also fuel the formation of an AGN (e.g. Hopkins et al. 2008, 2006). The discovery of massive reservoirs of molecular gas shifted far away from the quasar location has prompted some authors to suggest that gas poor/gas rich galaxy mergers can also trigger quasar activity (Riechers 2013, Aravena et al. 2011, Papadopoulos et al. 2008).

We are observing SDSS J0025-10 when the galaxies are deeply interpenetrating and approaching the final coalescence ( $r \lesssim$  a few kpc). Simulations of gas dynamics and starbursts in major gas rich mergers with or without quasar activity (e.g. Mihos & Hernquist 1996, Hopkins et al. 2005) show that at this stage the morphologies show distorted, irregular isophotes and extended tidal tails, as observed in SDSS J0025-10. The models also predict that at this moment the gas experiences the strongest levels of inflow so that large amounts of gas accumulate in the central region and very intense star formation activity is triggered as a consequence. The duration of the starburst is expected to be very short  $\sim 50$  Myr (Mihos & Hernquist 1994). The presence of such a young stellar population is confirmed in SDSS J0025-10 (see §1.1).

Sanders et al. (1988a) proposed that there is a natural evolution from ULIRG to QSO: ULIRGs are the initial dust-enshrouded stage of quasars, which will become optical quasars once the nuclei shed the obscuring dust via feedback mechanisms (see also Hopkins & Beacom 2005). Some authors have expanded the ULIRG-QSO evolutionary scenario accommodating luminous LIRGs as a phase that appears earlier in mergers than the ULIRG phase (e.g. Haan et al. 2011, Yuan, Kewley & Sanders 2010). A review on the observational and theoretical studies, with pros and cons of these scenarios can be found in the recent paper by Rothberg et al. (2013). Although the merger driven evolutionary sequence (U)LIRG-QSO probably is too simplistic (Veilleux et al. 2002), both theory and observations support that at least a significant fraction of optical quasars might evolve from a prior (U)LIRG phase.

In such scenario, SDSS J0025-10 is a strong candidate to be a (U)LIRG-optical QSO transition object. All the properties investigated here are expected for such a transition phase: high infrared luminosity powered by intense star formation, a rich molecular gas reservoir, strong evidence for a major merger of two gas rich progenitors and optical identification of quasar activity (Sanders et al. 1988a, 1988b).

The nuclear separation in SDSS J0025-10 ( $\sim 5$  kpc) is consistent with typical values of double nuclei LIRGs and significantly larger than in more advanced mergers (e.g. Haan et al. 2011, Yuan, Kewley & Sanders 2010), which are more frequently found in ULIRGs. This and the fact that a large fraction of the molecular gas is still unsettled show that the system is in an transient stage prior to the final coalescence of the nuclei.

The identification of an ionized outflow associated with the quasar nucleus (VM11b), prompts the interesting possibility of tracing its signature in both the neutral and molecular phases to fully characterize its mass, geometry and energetics. This information would allow to evaluate whether the outflow is powerful enough to clear up completely the material surrounding the quasar nucleus, quench the star formation activity and convert SDSS J0025-10 into an optical quasar before becoming a non active massive elliptical galaxy (e.g. di Matteo, Springel & Hernquist 2005).

#### 4.3 A large reservoir of molecular gas at the tip of the tidal tail

Merger simulations of gas rich galaxies show that, besides the infalling gas which concentrates in a compact central region of less than 1 kpc in size, part of the gas survives the merger (Barnes & Hernquist 1996; Mihos & Hernquist 1996; Hopkins et al. 2008). This is primarily material which has been moved to large radii temporarily, either blown out by a combination of supernova and AGN feedback or thrown out in tidal tails. The lack of spatial information prevents us from making a confident elucidation of the nature of J0025A and J0025B but given their spatial location, it is reasonable to propose that J0025A is (or will become) the compact component while J0025B, associated with the northern tidal tail, is “surviving” material.

In Fig. 4, it seems that the locations of the peak of the CO(1-0) emission in the various channel maps traces the tidal tail, from the inner spiral-like structure between the nuclei to the tip of the tail, maybe beyond. This sug-

gests that there is molecular gas along the tail. According to the model predictions, this surviving gas will then slowly settle back into a small, rotationally supported embedded disk (Hopkins et al. 2008, Bournaud & Duc 2006)  $\sim$  a couple  $\times 10^8$  yr after the coalescence. This gas is not expected to contribute much to the galaxy stellar mass ( $\sim$  a few per cent), even for the most gas rich mergers. Thus, although a large reservoir of gas is still falling towards the center, it seems unlikely that it will produce a significant enhancement on the build up of the galaxy stellar mass.

On the other hand, the centroid of J0025B is coincident with a prominent feature of elliptical shape located at the tip of the northern tidal tail and clearly identified in the HST image (Fig. 4). A CO accumulation at a tidal tail's tip is a promising tidal dwarf galaxy (TDG) candidate (Bournaud & Duc 2006). A TDG is a self-gravitating entity that was made up from the debris of a galaxy interaction.

Indeed, the properties of the optical feature strongly support this scenario. The optical size along the major axis  $D = 1.4 \pm 0.1$  kpc, the effective radius  $R_{eff} = 0.70 \pm 0.06$  kpc, the observed  $H\beta$  luminosity  $L(H\beta) = 3.6 \times 10^{40}$  erg  $s^{-1}$  (VM11a) are all consistent with values measured for TDGs (e.g. Monreal Ibero et al. 2007, Bournaud & Duc 2006). The J0025B CO(1-0) line luminosity is  $\gtrsim 50$  times higher (and therefore implies  $\gtrsim 50$  times more molecular gas mass) than typically measured for TDGs (e.g. Braine, Duc & Linsfeld 2001), but this most probably reflects the CO(1-0) contamination of J0025B by emission from other regions.

The dynamical mass of the TDG can be estimated as (Monreal Ibero et al. 2007):

$$M_{\text{dyn}}(M_{\odot}) = \text{constant} \times 10^6 \frac{R_{\text{eff}}}{\text{kpc}} \left( \frac{\sigma}{\text{km s}^{-1}} \right)^2$$

The *constant* value ranges between 1.4 and 2.2. Following Monreal Ibero et al. (2007) we adopt a value of 2.09. This calculation is highly uncertain due to the uncertainty on the exact mass distribution of the object and specially on the velocity dispersion  $\sigma = \text{FWHM}/2.35$ . In spite of this, an estimation of the ranges allowed can be useful to support or discard the TDG scenario. The  $\text{FWHM}_{\text{CO}} = 165 \pm 85$   $\text{km s}^{-1}$  of J0025B<sup>4</sup> is not a reliable tracer of the dynamical mass, since, as we have seen, it is contaminated by emission from other regions. On the other hand, the optical emission lines, which are much less affected by this problem, have  $\text{FWHM}(H\beta) \leq 140$   $\text{km s}^{-1}$ ,  $\text{FWHM}([\text{OIII}]\lambda 5007) = 330 \pm 10$   $\text{km s}^{-1}$  (VM11a) and  $\text{FWHM}([\text{OI}]\lambda 6300) = 140 \pm 20$   $\text{km s}^{-1}$ . Such discrepancy for [OIII] might indicate that it is broadened by some turbulent mechanism (e.g. winds). It is reasonable to assume  $\text{FWHM} \sim 140$   $\text{km s}^{-1}$  or  $\sigma \sim 60$   $\text{km s}^{-1}$  (notice that this value also locates the system with other TDGs in the  $R_{eff}$  vs.  $\sigma$  plane; e.g. Monreal Ibero et al. 2007). In such case,  $M_{\text{dyn}} \sim 5 \times 10^9 M_{\odot}$ . Dynamical masses as large as this have been measured for other TDG (Monreal Ibero et al. 2007, Bournaud & Duc 2006). At the lowest extreme, even unexpectedly small  $\sigma$  values (e.g. 10  $\text{km s}^{-1}$ ) would result

<sup>4</sup> This value is larger than  $80 \pm 40$   $\text{km s}^{-1}$  quoted in §3.2 for the red fainter component of the double horned CO profile. The reason is that the total CO emission associated with J0025B has been considered, rather than only the inner  $2.3'' \times 2.3''$  *pixel* used to build the 1-dimensional spectrum discussed in that section.

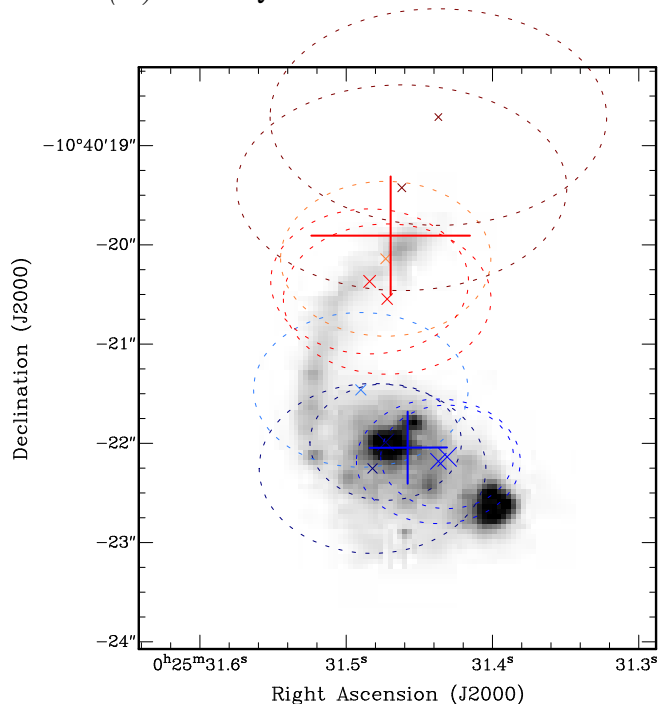


**Figure 4.** Overview of the location of the CO(1-0) peak emission against features seen in the HST image (grey-scale). The large ‘+’ signs indicate the location of the peak of the CO(1-0) emission in J0025A (blue) and J0025B (red) derived from the total intensity image of Fig. 3 (see text for details). The region covered by the size of the ‘+’ symbol indicates the uncertainty in the exact location as a result of uncertainty in the fitting of the CO(1-0) peak combined with astrometric uncertainty (§2). The crosses indicate the location of the peak of the CO(1-0) emission in the various channel maps of Fig. 3 (dark blue  $\rightarrow$  dark red for lowest  $\rightarrow$  highest velocities). The size of the cross scales with the significance level at which the CO(1-0) is detected, while the dashed ellipses indicate the uncertainty in the exact location (from the CO(1-0) fitting combined with astrometric errors). A color version of this figure can be seen in the electronic form.

in  $M_{\text{dyn}} > 10^8 M_{\odot}$ , still typical of TDGs. Thus, in spite of the uncertainties, we confirm that the dynamical mass of the optical tidal feature associated with J0025B centroid is in the range of TDGs.

The formation of such massive self-gravitating condensations of matter in the outer regions of tidal tails is allowed by the simulations, without strong constraints on the galactic encounter parameters (Bournaud & Duc 2004). These condensations can survive longer ( $> 1$  Gyr) than the inner regions of the tails. According to these simulations, only the objects formed at the tip of tidal tails can become long-lived, massive, dwarf satellite galaxies. Whether this will be the case depends on its stability against its own internal motions and against tidal forces from the parent galaxies.

## 5 SUMMARY AND CONCLUSIONS

We have characterized the amount, spatial distribution and kinematics of the molecular gas in the optically selected type 2 quasar SDSS J0025-10 at  $z = 0.30$ , which is a merging system with a double composite nucleus (AGN+HII). For this, we have used the CO(1-0) transition based on data obtained

with the Australia Telescope Compact Array (ATCA). This is one of the scarce examples of quasar host galaxies where the CO emission has been resolved spatially at any redshift.

The system contains  $M_{\text{H}_2}=(6\pm 1)\times 10^9 M_{\odot}$ , which is distributed in two main reservoirs separated by  $\sim 9$  kpc.  $\sim 60\%$  of the gas is in the central region, preferentially associated with the QSO nucleus and/or the intermediate region between the two nuclei. The other 40% is associated with the northern tidal tail and is therefore unsettled.

Based on WISE and IRAS photometry, we constrain the infrared luminosity  $L_{\text{IR}}=(1.1\pm 0.3)\times 10^{12} L_{\odot}$  and show that it is dominated by a starburst, rather than the AGN. SDSS J0025-10 is an analogue of local ( $z \lesssim 0.05$ ) luminous LIRGs and ULIRGs. The clear morphological evidence for an ongoing major merger, the large molecular gas content, the star forming rate  $\text{SFR}=190\pm 52 L_{\odot} M_{\odot}^{-1}$ , the star formation efficiency  $\text{SFE}=183\pm 62 L_{\odot} M_{\odot}^{-1}$  and the gas exhaustion time scale  $\tau_{\text{SF}} = 32\pm 11$  Myr are all in the range of these local systems.

SDSS J0025-10 is the result of an ongoing major merger of two gas rich progenitors. This, together with the high infrared luminosity dominated by a starburst, the massive reservoir of molecular gas and the quasar activity are all properties consistent with a transition phase in the (U)LIRG-optical QSO evolutionary scenario. The relatively large nuclear separation ( $\sim 5$  kpc) and the existence of large amounts of unsettled molecular gas (probably surviving gas from the merger), moreover suggest that we are observing the system during a particular transient phase, prior to more advanced mergers where the nuclei have already coalesced.

We propose that at least part of the extended, unsettled reservoir of molecular gas is associated with a tidal dwarf galaxy at the tip of the northern tidal tail identified in the HST image. The formation of tidal dwarf galaxies in the outer regions of tidal tails is predicted by simulations of colliding galaxies.

## ACKNOWLEDGMENTS

Thanks to an anonymous referee for useful comments that helped improve the paper substantially. Thanks to Luis Colina for useful discussions and suggestions on the manuscript.

This work has been funded with support from the Spanish former Ministerio de Ciencia e Innovación through the grant AYA2010-15081. ATCA is funded by the Commonwealth of Australia for operation as a National Facility managed by CSIRO.

## REFERENCES

- Alonso Herrero A., 2013, to appear in *Nuclei of Seyfert galaxies and QSOs - Central engine and conditions of star formation*. Proceedings of Science
- Aravena M., Wagg J., Papadopoulos P., Feain I., 2011, *ApJ*, 737, 64
- Barnes J.E., Hernquist L., 1996, *ApJ*, 471, 115
- Bertram T., Eckart A., Fischer S., Zuther J., Straubmeier C., Wisotzki L., Krips M., 2007, *A&A*, 470, 571
- Bessiere P., Tadhunter C., Ramos Almeida C., Villar Martín M., 2012, *MNRAS*, 426, 276
- Bournaud F., Duc P.A., Amram P., Combes F., Gach J.L., 2005, *A&A*, 425, 813
- Bournaud F., Duc P.A., 2006, *A&A*, 456, 481
- Briggs D. S., 1995, PhD thesis, New Mexico Tech
- Braine J., Duc P., Linsfeld U., Charmandaris V., Vallejo O., Leon S., Brinks E., 2001, *A&A*, 378, 51
- Bryant P. M., Scoville N. Z., 1999, *AJ*, 117, 2632
- Carilli C., Cox P., Bertoldi F. et al., 2002, *ApJ*, 575, 145
- Carilli C., Daddi E., Riechers D. et al., 2010, *ApJ*, 714, 1407
- Di Matteo T., Springel V., Hernquist L., 2005, *Nature*, 433, 605
- Downes D., Solomon P., 1998, *ApJ*, 507, 615
- Emonts B., Norris R., Feain I. et al. 2011, *MNRAS*, 415, 655
- Feruglio C., Maiolino R., Piconcelli E., Menci N., Aussel H., Lamastra A., Fiore F., 2010, *A&A*, 518, L155
- Haan S., Surace J., Armus L. et al., 2011, *AJ*, 141, 100
- Hopkins P. F., Hernquist L., Martini P., Cox T. J., Robertson B., Di Matteo T., Springel V., 2005, *ApJ*, 625, L71
- Hopkins P., Beacom J., 2006, *ApJ*, 651, 142
- Hopkins P., Hernquist L., Cox T., Dutta S.N., Rothberg B., 2008, *ApJ*, 679, 156
- Kennicutt R., 1998, *ARA&A*, 36, 189
- Krips M., Eckart A., Neri R., Bertram T., Straubmeier C., Fischer S., Staguhn J.G., Vogel S.N., 2007, *A&A*, 464, 187
- Krips M., Neri R., Cox P., 2102, *ApJ*, 753, 135
- Martínez Sansigre A., Karim A., Schinnerer E. et al., 2009, *ApJ*, 706, 184
- Middelberg E., Sault R., Kesteven M., 2006, *PASA*, 23, 147
- Mihos J.C., Hernquist L., 1994, *ApJ*, 431, L9
- Miralles-Caballero D., Colina L., Arribas S., Duc P.A., 2011, *AJ*, 142, 79
- Monreal-Ibero A., Colina L., Arribas S., Garca-Marín M., 2007, *A&A*, 472, 421
- Nardini E., Risaliti G., Watabe Y., Salvati M., Sani E. 2010, *MNRAS*, 405, 2505.
- Norris R. P., Mao M. Y., Lenc E., Emonts B., Sharp R. G., 2013, in "The Interstellar Medium in High Redshift Galaxies Comes of Age", NRAO Conference Series, Vol. 28, ed. J. G. Mangum
- Papadopoulos P., Ivison R., Carilli C., Lewis G., 2001, *Nature*, 409, 58
- Papadopoulos P., Feain I., Wagg J., Wilner D., 2008, *ApJ*, 648
- Polletta M., Weedman D., Hönig S., Lonsdale C., Smith H., Houck J., 2008, *ApJ*, 675, 960
- Ramos Almeida C., Bessiere P., Tadhunter C., Pérez-González P. G., Barro G., Inskip K. J., Morganti R., Holt J., Dicken D., 2011, *MNRAS*, in press
- Riechers D., 2013, *ApJL*, in press
- Robitaille P., Whitney B., 2010, *ApJ*, 710, 11
- Rodríguez-Zaurín J., Arribas S., Monreal-Ibero A., Colina L., Alonso-Herrero A., Alfonso-Garzón J., 2011, *A&A*, 527, 60
- Rothberg B., Fischer J., Rodrigues M., Sanders D.B., 2013, *ApJ*, in press
- Sanders D.B., Soifer T.B., Elias J.H., Madore B.F., Matthews K., Neugebauer G., 1988a, *ApJ*, 325, 74
- Sanders D.B., Soifer T.B., Elias J.H., Neugebauer G., Matthews K., 1988b, *ApJ*, 328, L35
- Sanders D.B., Phinney E.S., Neugebauer G., Soifer B.T.,



- Matthews K., 1989, *ApJ*, 347, 29
- Sanders D.B., Mirabel F., 1996, *ARA&A*, 34, 749
- Sault R., Teuben P., Wright M., 1995, *ASPC*, 77, 433
- Solomon P., Vanden Bout P., 2005, *ARA&A*, 43, 677
- Staguhn J., Schinnerer E., Eckart A., Scharwächter J., 2004, *ApJ*, 609, 85
- Tacconi L., Genzel R., Tezcla M., Gallimore J.F., Downes D., Scoville Z., 1999, *AJ*, 524, 732
- Tecza M., Genzel R., Tacconi L., Anders S., Tacconi-Garman L., Thatte N., 2000, *ApJ*, 537, 178
- Tadhunter C., Holt J., González Delgado R. et al. 2011, *MNRAS*, 412, 960
- Toomre A., Toomre J., 1977, *ApJ*, 178, 623
- Vernet J., Fosbury R. A. E., Villar-Martín M., Cohen M. H., Cimatti A., di Serego Alighieri S., Goodrich R. W., 2001, *A&A*, 366, 7
- Veilleux S., Kim D.C., Sanders D. B., Mazzarella J. M., Soifer B. T., 1995, *ApJS*, 98, 171
- Veilleux S., Kim D.C., Sanders, D. B., 1999, *ApJ*, 522, 113
- Veilleux S., Kim D.C., Sanders D.B., 2002, *ApJS*, 143, 315
- Westmoquette M.S., Clements D.L., Bendo G.J., Khan S.A., 2012, *MNRAS*, 424, 416
- Villar-Martín M., Tadhunter C., Humphrey A., Fraga Encina R., González Delgado R., Pérez Torres M., Martínez-Sansigre A., 2011a, *MNRAS*, 416, 262 (VM11a)
- Villar-Martín M., Humphrey, A., González Delgado R., Colina L., Arribas S., 2011b, *MNRAS*, 418, 2032 (VM11b)
- Villar-Martín, M., Cabrera Lavers, A., Bessiere, P., Tadhunter C., Rose M., de Breuck C., 2012, *MNRAS*, 423, 80
- Villar-Martín M., Rodríguez, Drouart G. et al., 2012, *MNRAS*, submitted
- Xia X. Y., Gao, Y., Hao C.-N. et al., 2012, *ApJ*, 750, 92
- Yuan T.T., Kewley L.S., Sanders D.B., 2010, *ApJ*, 709, 884
- Zakamska N., Strauss M., Krolik J. et al. 2003, *AJ*, 126, 2125